Intensification and Kinetics of Methane Hydrate Formation Under Heat Removal by Phase Change of *n*-Tetradecane

Xiaofei Song, Feng Xin, Hongchao Yan, Xingang Li, and Hongri Jia
School of Chemical Engineering and Technology, Tianjin University, Tianjin 300072, China

Collaborative Innovation Center of Chemical Science and Engineering (Tianjin), Tianjin 300072, China

DOI 10.1002/aic.14867
Published online May 19, 2015 in Wiley Online Library (wileyonlinelibrary.com)

A method of direct heat removal resulting from the phase change of n-tetradecane was used to intensify the heat transfer during hydrate formation. The growth rates of methane hydrate in aqueous slurries containing 25–45 wt % of solid n-tetradecane were investigated at pressures between 4.70 and 6.46 MPa (gauge) and near the fusion point of solid n-tetradecane. Methane hydrate growth started at a practically constant rate, which became variable after a sudden increase. Two rate laws were established to correlate with the experimental data for the constant and variable rate stages. The methane hydrate growth rates achieved with solid n-tetradecane were significantly enhanced compared with those obtained under indirect heat removal. © 2015 American Institute of Chemical Engineers *AIChE J*, 61: 3441–3450, 2015

Keywords: methane hydrate formation, kinetics, model, phase change emulsion, heat removal

Introduction

Gas hydrates are crystalline clathrates formed by small guest molecules and water molecules under specific pressure and temperature ranges. Gas hydrates have been intensively researched in recent years for their applications in gas storage,[1,2] sequestration of carbon dioxide,[3,4] gas separation,[5] and desalination of sea water.[6] A sufficient understanding of the kinetics of hydrate formation is necessary for these promising applications.

Many models of hydrate-growth kinetics have already been proposed. Based on the crystallization theory and two-film theory, Englezos et al.[7,8] established an intrinsic kinetic model for hydrate formation in pure water at minimized mass- and heat-transfer resistances by strongly agitating the aqueous phase. Using the experimental results of Englezos et al.,[8] Skovborg and Rasmussen[9] developed a simplified model assuming that the hydrate growth rate was controlled by the transfer of methane from the gas phase to the water phase. Turner et al.[10] proposed a shell growth model for hydrate formation in water-in-oil dispersions and hypothesized that the mass transfer of gas through the hydrate shell was the rate-determining step. Mochizuki and Mori[11] considered that the lateral growth rate of a hydrate film along a water/hydrate-forming fluid interface was controlled by the heat transfer in their rate laws.

Hydrate formation is an exothermic process. The large amount of heat released (54.44 ± 1.45 kJ/mol methane)[12] must be quickly removed; otherwise, the formation of hydrate will slow down and finally cease. Indirect and direct methods for removing the heat exist in the literature. Most investigators immersed hydrators in low-temperature baths or equipped hydrators with cooling jackets to remove the heat indirectly. Pang et al.[13] placed coiled copper tubes inside a hydrator to enhance the heat transfer. Yang et al.[14] investigated hydrate formation in a tubular finned heat exchanger. However, in indirect heat exchange, the area available for heat transfer and the coefficient of heat transfer are limited compared with those of direct heat exchange. Furthermore, the built-in heat exchanger would complicate the scale-up of an industrial hydrator. Direct heat removal has been realized by the phase changes of ice powders,[15,16] chlorofluorocarbon (CFC) alternatives,[17] and dichlorodifluoromethane (R12).[18] Nevertheless, making ice is energy intensive and difficult under continuous operation conditions because of the cryogenic freezing of water on the tube surface of the heat exchanger; meanwhile, the hydrate-forming temperature is limited by the ice point. The CFC alternatives and R12, as hydrate formers, must be liquefied and then vaporized to remove the heat, which is unsuitable for most of the hydrate-forming gases such as methane and ethane.

Phase change emulsions (PCEs) consist of phase change materials (PCMs) as dispersed phases and carrier fluids as continuous phases. PCEs possess many excellent properties. First, the PCM in a PCE can store a large quantity of heat during an approximately isothermal phase change.[19,20] In addition, the dispersed PCM has a large surface-to-volume ratio.[19] Furthermore, some properly prepared PCEs can be pumped during their phase transitions.[21] In particular, the phase-change temperature of paraffin, a typical PCM, varies with the number of carbon atoms in its chain.[20] The solid particles and droplets of paraffin can induce hydrate nucleation and absorb more organic gas than water, respectively. Until now, gas hydrate formation in a slurry containing solid particles of paraffin has

Correspondence concerning this article should be addressed to F. Xin at xinf@tju.edu.cn.

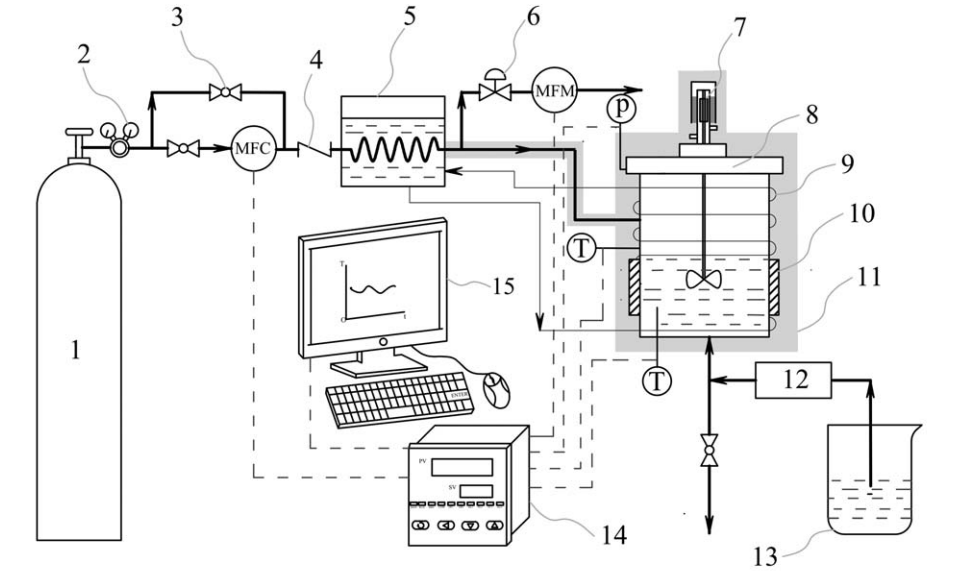

Figure 1. Schematic diagram of the experimental setup.

not been described in the literature. In this work, liquid *n*-tetradecane was dispersed in water to form o/w emulsions, which were transformed to slurries after being frozen. Methane hydrate formation occurred in the slurries near the fusion point of solid *n*-tetradecane.

Experimental Section

Apparatus and materials

The hydrator (inner diameter, 35 mm; height, 60 mm; volume, 50 cm^3) in Figure 1 was made of 316 L stainless steel. A magnetic driver and two sapphire windows were installed on the top and the opposite sides of the hydrator, respectively. Copper tubes through which a chilled aqueous solution of ethylene glycol was forced to flow were tightly twisted around the hydrator. The hydrator, as well as the inlet tube between the hydrator and a low-temperature thermostat, was insulated with polyurethane foam. By adjusting the temperature and flow rate of the aqueous solution of ethylene glycol, the external temperature of the hydrator—namely, the temperature between the hydrator and the polyurethane foam—could be controlled. Two Pt100 resistance temperature detectors with a precision of ± 0.1 K were used to monitor the internal and external temperatures of the hydrator. Methane was precooled to the fusion point of solid *n*-tetradecane in the low-temperature thermostat prior to entering the hydrator. The pressure in the hydrator was detected and controlled by a pressure transducer (CYB-20S, Beijing WESTZH Machine and Technology) and a backpressure valve (K9138F-1P-B, Beijing Xiongchuan Valve Manufacturing Co.). The measurement uncertainties of both the pressure transducer and the backpressure valve were 10 kPa. The temperatures, pressures, and gas flow rates were shown on a secondary instrument and recorded by computer software. The PCE was prepared using a high-performance disperser (T25 digital ULTRA-TURRAX, IKA-Labortechnik).

Methane ($\geq$99.99 wt %) was purchased from Liufang Gas Company, Tianjin. Chemically pure sorbitane monooleate (Span 80) and polyoxyethylene sorbitan monostearate (Tween 60) were obtained from Guangfu Chemical Plant, Tianjin. Both Span 80 and Tween 60 were surfactants used for stabilizing the PCE. *n*-Tetradecane ($\geq$98 wt %) was obtained from Aladdin Company.

Preparation of the PCE

The fraction of *n*-tetradecane in the PCE was selected to be in the range of 25–45 wt % by striking a balance between the energy density and viscosity of the slurry. The two-step procedure for preparing the PCE was to first precisely weigh Tween 60, Span 80, *n*-tetradecane, and deionized water according to the proportion shown in Table 1. Then, the mixture of them was emulsified at a rotation speed of 10,000 rpm for 5 min using the high-performance disperser. The size distribution of the PCE was analyzed using a Malvern Mastersizer 3000. The fusion point of solid *n*-tetradecane in the slurry transformed from the PCE was measured using a Netzsch DSC 200F3 with a scanning rate of 2 K/min from 263.2 to 283.2 K.

Hydrate formation

Prior to hydrate formation, the mass flow meter (MFM), mass flow controller (MFC), and pressure and temperature sensors in Figure 1 were calibrated. The hydrator and the inlet tubes were successively rinsed with deionized water and the prepared PCE. The system was then purged with methane to expel air. Subsequently, 16 cm^3 of the PCE was pumped into the hydrator, and the low-temperature thermostat was started to cool down the hydrator. After complete transformation of the *n*-tetradecane droplets in the PCE into solid particles, the

Table 1. Compositions and Properties of the Prepared PCEs

Type	Deionized Water (wt %)	*n*-Tetradecane (wt %)	Tween 60 (wt %)	Span 80 (wt %)	Median Diameter (μm)	Fusion Point[a] (K)
1#	71	25	2.92	1.08	3.655	276.6
2#	61	35	2.92	1.08	3.680	276.6
3#	51	45	2.92	1.08	3.429	276.6

[a]Fusion point is for the slurry transformed from the PCE.

obtained slurry was heated to a temperature slightly below the fusion point listed in Table 1. Next, the hydrator was quickly pressurized with methane to the desired pressure. Once the system pressure was stabilized, the impeller rotation was started, and the software began to record the temperatures, pressures, and gas flow rates every 5 s. Methane was continuously supplied to the hydrator for an isobaric operation during hydrate formation. The formation of hydrate was continued until the difference in the instantaneous value between the MFC and the MFM approached zero.

Data Interpretation

Methane absorbed by water during the induction period

It was assumed that the methane in the hydrator was not absorbed by water in the short time period before the impeller rotation was started. After starting the rotation of the impeller, the enlargement of the methane-water interfacial area prompted methane absorption in water and hydrate nucleation within a few minutes, which is called the induction period. The heat released by the methane absorption in water in this period is supposed to be too small to fuse the solid particles of *n*-tetradecane in the slurry because the solubility of methane in water is several orders of magnitude smaller than that in oil.[10] Then, the moles of methane absorbed by water can be determined as follows

$$(n)_{\mathrm{w}} = n_{\mathrm{MeC}} - n_{\mathrm{MeM}} \tag{1}$$

where $(n)_{\mathrm{w}}$ is the moles of methane absorbed by water, n_{MeC} is the moles of methane that flowed through the mass flow controller, and n_{MeM} is the moles of methane that flowed through the mass flow meter.

Methane enclathrated in hydrates

Assuming that the fused *n*-tetradecane in the slurry was always saturated with methane, a mole balance and a heat balance were established to quantify the methane enclathrated in hydrates during hydrate growth.

Figure 2a shows the mass transfer in the hydrator. Only the structure I hydrate is supposed to be formed in this work. As stated by Parrish and Prausnitz,[22] for the structure I hydrate, the molar volume of the imaginary empty hydrate lattice is 4.6 cm^3 larger than that of water, which indicates that the volume of water expands approximately 1.25 times after it is converted into the hydrate. The quantity of methane released from the consumed water is negligible compared with that consumed due to absorption in the fused *n*-tetradecane and enclathration in hydrates during hydrate growth. The conservation of the total quantity of methane confined in the hydrator during hydrate growth is thus expressed as

$$(n)_{\mathrm{o}} + (n)_{\mathrm{h}} = n_{\mathrm{MeC}} - n_{\mathrm{MeM}} + \frac{0.25(n)_{\mathrm{h}} P N M_{\mathrm{w}}}{ZRT\rho_{\mathrm{w}}} \tag{2}$$

where $(n)_{\mathrm{o}}$ is the moles of methane absorbed by liquid *n*-tetradecane; $(n)_{\mathrm{h}}$ is the moles of methane enclathrated in hydrates; P and T are the experimental pressure and temperature, respectively; and M_{w} and ρ_{w} are the molecular weight and density of water, respectively. The hydration number N was obtained from Tulk et al.[23] The third term on the right-hand side of Eq. 2 represents the decrease in moles of methane in

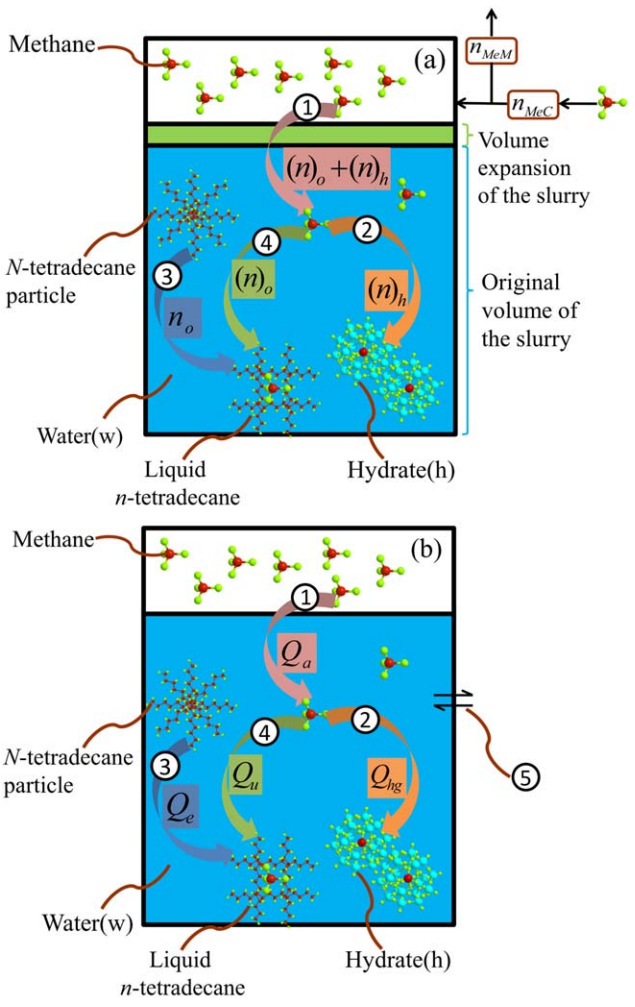

Figure 2. Schematic diagram of the mass transfer (a) and heat flow (b) during hydrate growth.

[Color figure can be viewed in the online issue, which is available at wileyonlinelibrary.com.]

the gas phase due to its shrinkage caused by the volume-expanding conversion of water to hydrate.

Figure 2b shows the heat flows in the hydrator. We define the entire volume of the slurry inside the hydrator as the control volume on which the heat balance is to be formulated. In the figure, there is heat released from the absorption of methane into water, Q_a; heat released from the formation of methane hydrate, Q_{hg}; heat released from the fusion of solid *n*-tetradecane, Q_e; heat absorbed by the transfer of methane from the water to the liquid *n*-tetradecane, Q_u; sensible heat of the slurry and heat exchange between the slurry and the hydrator wall.

The calculations of the above heat flows are as follows

$$Q_a = -\left((n)_o + (n)_h\right)\Delta H_a \tag{3}$$

The molar enthalpy change of methane due to its absorption into water, ΔH_a, was obtained from Naghibi et al.[24]

$$Q_{hg} = -(n)_h \Delta H_{hg} \tag{4}$$

where ΔH_{hg} is the change in enthalpy per mole of methane due to its enclathration in hydrates

$$Q_e = n_o \Delta H_e \tag{5}$$

where n_o is the moles of liquid *n*-tetradecane and ΔH_e is the molar enthalpy change of fusion of solid *n*-tetradecane

$$Q_u = (n)_o \Delta H_u \tag{6}$$

where ΔH_u is the molar enthalpy change of methane caused by its transfer from the water to liquid *n*-tetradecane.

The sensible heat of the slurry was regarded to be zero because its temperature was almost constant.

The heat transfer between the slurry and the hydrator wall was determined to be negligible if the external temperature of the hydrator was kept at approximately the fusion point of solid *n*-tetradecane during hydrate formation. The test was carried out as follows. The prepared PCE (16 cm^3) was pumped into the hydrator and cooled down using the hydrate-forming agitation speed. The external temperature of the hydrator was controlled at the fusion point of solid *n*-tetradecane. The decrease in the PCE temperature over 1 h was less than 0.2 K when the temperature difference between the inside and the outside of the hydrator approached zero. This result suggests that the rate of heat transfer from the PCE to the wall of the hydrator is sufficiently low.

The general heat balance is

$$Q_a + Q_{hg} = Q_e + Q_u \tag{7}$$

Substituting Eqs. 3–6 into Eq. 7 yields

$$\left((n)_o + (n)_h\right)\Delta H_a + (n)_h \Delta H_{hg} + n_o \Delta H_e + (n)_o \Delta H_u = 0 \tag{8}$$

The molar ratio of methane to *n*-tetradecane in the *n*-tetradecane solution saturated with methane under the experimental pressure and temperature, *D*, can be obtained from the thermodynamic flash calculation.[25] As assumed previously, *D* is

$$D = \frac{(n)_o}{n_o} \tag{9}$$

Combining Eqs. 2, 8, and 9, the moles of methane enclathrated in hydrates $(n)_h$ can be calculated.

Rate of hydrate growth

The rate of hydrate growth, r_{hg}, is defined as

$$r_{hg} = \frac{1}{V_w^0}\frac{d(n)_h}{dt} \tag{10}$$

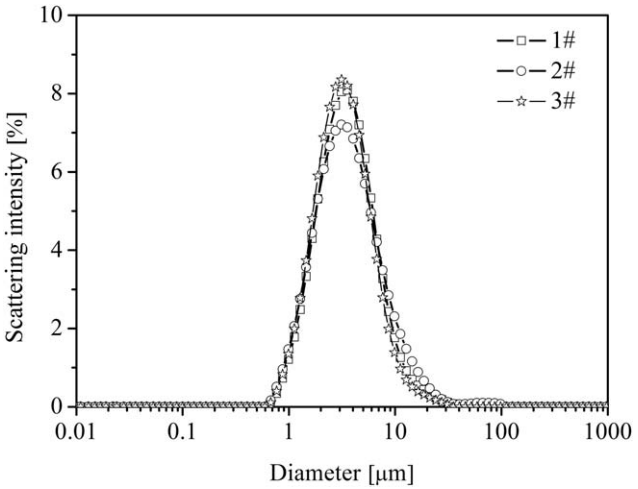

Figure 3. Size distributions of the *n*-tetradecane droplets in the 1#, 2#, and 3# PCEs.

where V_w^0 is the volume of water in the slurry at the onset of hydrate growth. The time interval for the calculation of the derivative is 20 s.

Volume fraction of water in the slurry

Using Eqs. 11 and 12, the volume fraction of water in the slurry, φ, can be calculated

$$\varphi = \frac{V_w}{V_w + V_o} \times 100 \tag{11}$$

$$V_w = V_w^0 - \frac{(n)_h N M_w}{\rho_w} \tag{12}$$

where V_w and V_o are the volumes of water and liquid *n*-tetradecane in the slurry, respectively.

Degree of deviation from equilibrium

The degree of deviation from equilibrium, *F*, was defined to facilitate the comparison of hydrate growth rates in this work with those in the literature because both pressure and temperature influence the rates.

$$F = P/P^{eq} \tag{13}$$

The methane-water-hydrate equilibrium pressure under the experimental temperature, P^{eq}, was calculated using the method proposed by Ballard and Sloan.[26]

Results and Discussion

Properties of the prepared PCEs

In Figure 3 and Table 1, the sizes and median diameters of the *n*-tetradecane droplets were in the ranges of 0.6–100 and 3.429–3.680 μm, respectively, in the 1#, 2#, and 3# PCEs. This result indicated that the mass fraction of *n*-tetradecane had little influence on the size distribution of the *n*-tetradecane droplets in the PCE.

Figure 4 shows a part of the temperature profile for the 3# PCE cooled in the hydrator prior to hydrate formation. As shown, the temperature remained between 272.1 and 272.3 K for a relatively long time period. This phenomenon suggested that the *n*-tetradecane droplets mainly solidified at temperatures between 272.1 and 272.3 K. Finally, the temperature quickly decreased to 271.7 K, at which the *n*-tetradecane

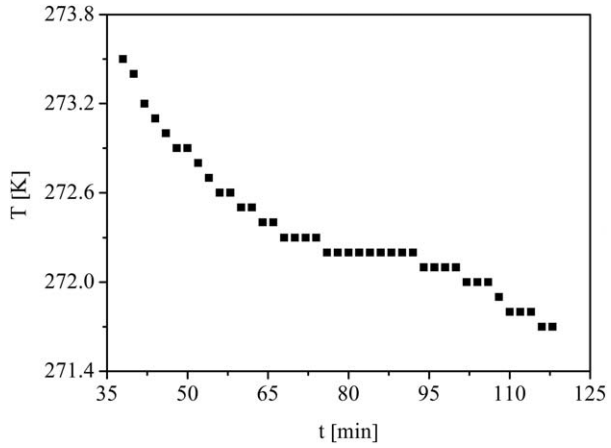

Figure 4. A part of the temperature profile for the 3# PCE cooled in the hydrator prior to hydrate formation.

droplets were considered to be fully transformed to solid particles. Note that only the *n*-tetradecane droplets underwent the phase change, whereas the water remained in the liquid state during this cooling process. The water in the PCE was frozen into a block rather than into small solid particles when chilled to 271.2 K. The temperature profiles for the 1# and 2# PCEs are similar to that for the 3# PCE.

In Figure 5, the fusion points—namely, the intersections between the tangents to the maximum rising slopes of the peaks and the extrapolated sample baselines[27]—of the solid particles of *n*-tetradecane in the 1#, 2#, and 3# slurries transformed from the corresponding PCEs were all 277.6 K. Roy and Avanic[28] noted that the slurry partly fused when maintained at its fusion point. Therefore, methane was introduced into the hydrator when the slurry was heated to a temperature slightly lower than the measured fusion point. Here, this temperature was chosen to be 277.1 K.

Gas consumption during hydrate formation

Figure 6 displays a typical curve for methane consumption vs. time as the result of absorption in water and enclathration in hydrates after starting the rotation of the impeller. A small

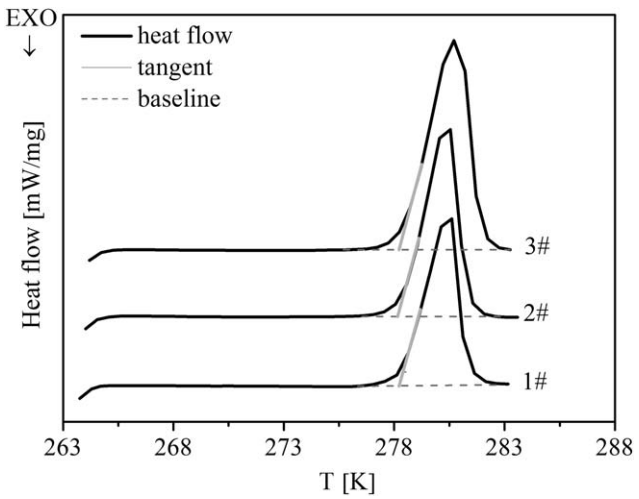

Figure 5. DSC heating curves for the 1#, 2#, and 3# slurries transformed from the corresponding PCEs.

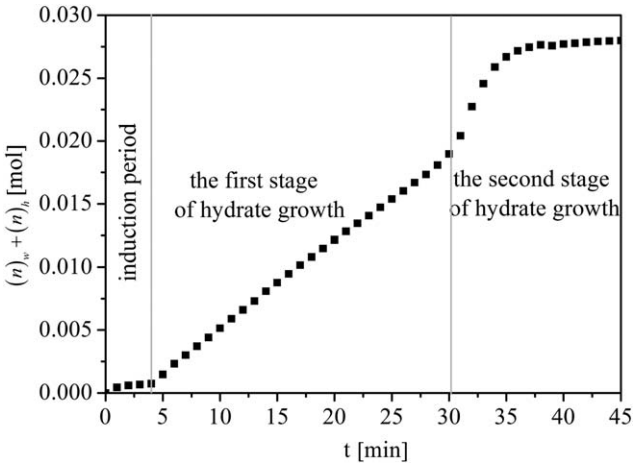

Figure 6. Methane consumption vs. time due to methane absorption in water and enclathration in hydrates after starting the rotation of the impeller (ψ =45 wt %; P =5.50 MPa (gauge); T =~277.6 K; impeller speed = 600 rpm).

amount of methane was quickly absorbed by water, and the nucleation of hydrates occurred in the first 4 min. This process represents the induction period. Apparently, the growth period in Figure 6 consisted of two stages. The hydrate grew at a practically constant rate in the first stage. A sudden increase in the growth rate identified the onset of the second stage, during which the growth rate varied with time and eventually approached zero.

To account for the sudden increase in the growth rate, the volume fractions of water in the slurries at the end of the first stage for various experimental conditions were calculated using Eq. 11 and are shown in Figure 7. The volume fractions in the 3# slurry were all ~46% except for the one at 6.46 MPa (gauge). It is thus considered that an inversion of the continuous phase in the slurry from the water to the liquid *n*-tetradecane occurred on account of the continuous consumption of water and the increase in the fused *n*-tetradecane. The inversion enhanced the transfer of methane in the gas phase to the water phase and increased the driving force for hydrate growth, leading to a faster growth rate. Furthermore, the

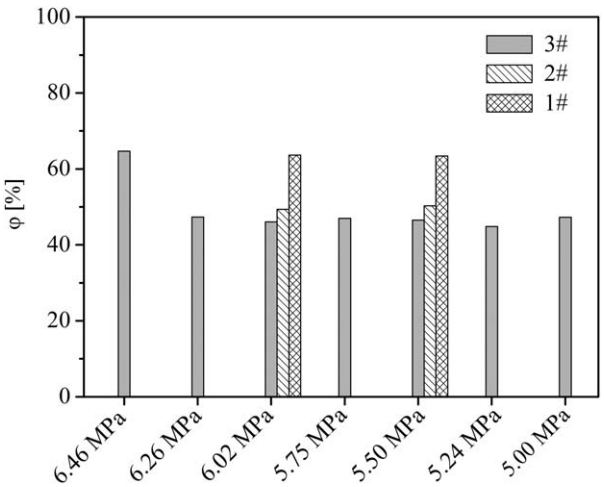

Figure 7. Volume fractions of water in the 1#, 2#, and 3# slurries at the end of the first stage under various pressures (T =~277.6 K; impeller speed = 600 rpm).

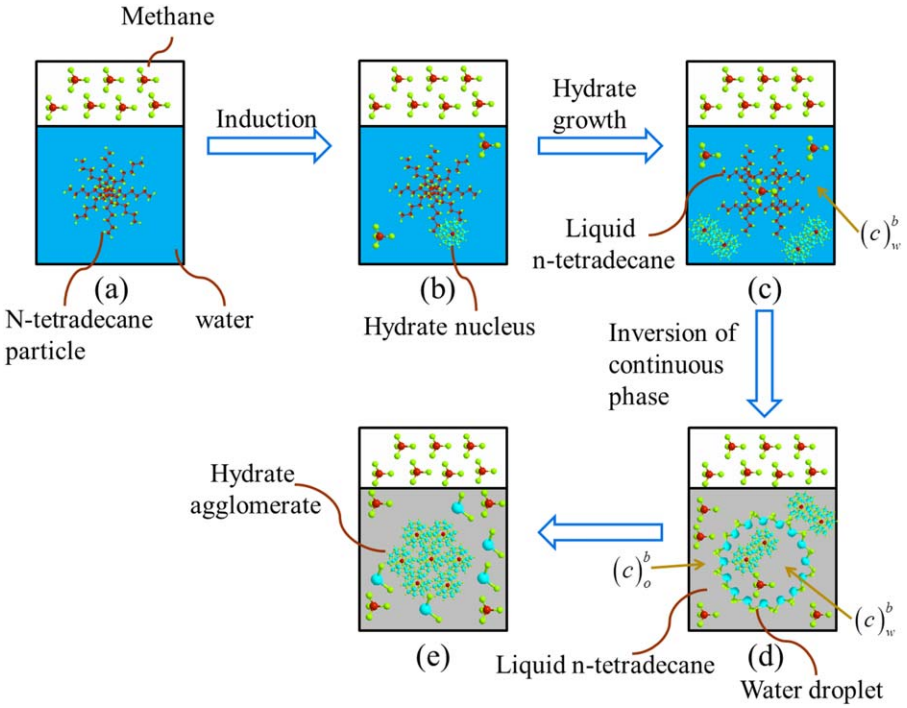

Figure 8. Illustration of the mechanism of hydrate formation.

[Color figure can be viewed in the online issue, which is available at wileyonlinelibrary.com.]

calculated volume fraction in Figure 7 was higher in the slurry initially containing more water. This result was likely due to more serious agglomeration of hydrates, in which more water was included. The actual volume fractions of water in the three groups of slurries were deemed to be the same when the inversions occurred.

Modeling of hydrate-growth kinetics

Based on the experimental results, the following hydrate formation mechanism was hypothesized; the mechanism is illustrated in Figure 8. Hydrate nuclei are first formed on the surfaces of solid particles of *n*-tetradecane. The nuclei subsequently grow while the solid particles of *n*-tetradecane continuously fuse by absorbing the released heat. The formed hydrates do not exist as shells encapsulating the solid particles of *n*-tetradecane; otherwise, the sudden increase in the growth rate is impossible. After the inversion of the continuous phase, the hydrates in water droplets grow at a different rate. Finally, the formed hydrates severely agglomerate, and hydrate formation tends to cease.

Two different models were established for the first and second stages of hydrate growth. The models exclusively consider the effect of the mass-transfer-dependent crystal growth on the hydrate-growth rate, based on the assumption that the heat released by the hydrate formation is immediately removed by the phase change of the PCM distributed in the slurry and that the heat transfer is no longer the rate-controlling factor of the hydrate growth.

In the first stage, the hydrate growth rate can be expressed by Eq. 14 by considering the mass transfer in the hydrator.

$$r_{\mathrm{hg}} = r_{\mathrm{a}} - D r_e \tag{14}$$

where r_{a} is the methane absorption rate in water and r_e is the fusion rate of solid particles of *n*-tetradecane.

The absorption rate is given by

$$r_{\mathrm{a}} = k_{\mathrm{a}} A^{\mathrm{g-w}} \left((c)_{\mathrm{w}}^{\mathrm{sat}} - (c)_{\mathrm{w}}^{\mathrm{b}} \right) \tag{15}$$

where k_{a} is the mass-transfer coefficient of methane absorption in water, $A^{\mathrm{g-w}}$ is the methane-water interfacial area per unit volume of water, $(c)_{\mathrm{w}}^{\mathrm{sat}}$ is the saturation concentration of methane in water at the experimental pressure and temperature, and $(c)_{\mathrm{w}}^{\mathrm{b}}$ is the concentration of methane in the bulk water.

Once released, the heat is supposed to be absorbed by the solid particles of *n*-tetradecane. Then

$$r_e = \frac{-r_{\mathrm{hg}} \Delta H_{\mathrm{hg}} - r_{\mathrm{a}} \Delta H_{\mathrm{a}} - r_u \Delta H_u}{\Delta H_e} \tag{16}$$

where r_u is the transfer rate of methane from the water to the liquid *n*-tetradecane.

According to the crystal growth theory of Karpinski,[29] the rate of hydrate growth can be formulated as Eq. 17 if the mass transfer at the diffusional layer around the hydrate particle is ignored

$$r_{\mathrm{hg}} = k_{\mathrm{hg}} A^{\mathrm{p}} \left((c)_{\mathrm{w}}^{\mathrm{b}} - (c)_{\mathrm{w}}^{\mathrm{eq}} \right) \tag{17}$$

where k_{hg} is the kinetic constant of methane hydrate growth, A^{p} is the surface area of hydrate particles per unit volume of water, and $(c)_{\mathrm{w}}^{\mathrm{eq}}$ is the methane saturation concentration in water under the methane-water-hydrate equilibrium. This equilibrium is assumed to occur at the experimental temperature and the corresponding methane-water-hydrate equilibrium pressure because the difference between the actual temperature of the formed hydrate particle and the experimental temperature is minimized using the PCM to intensify the heat removal.

Combining Eqs. 14–17, Eq. 18 can be derived

$$r_{\mathrm{hg}} = \frac{(c)_{\mathrm{w}}^{\mathrm{sat}} - (c)_{\mathrm{w}}^{\mathrm{eq}}}{\frac{1}{k_{hg} A^{\mathrm{p}}} + \frac{\Delta H_e + D\Delta H_u - D\Delta H_{\mathrm{hg}}}{\Delta H_e + D\Delta H_u + D\Delta H_{\mathrm{a}}} \cdot \frac{1}{k_{\mathrm{a}} A^{\mathrm{g-w}}}} \tag{18}$$

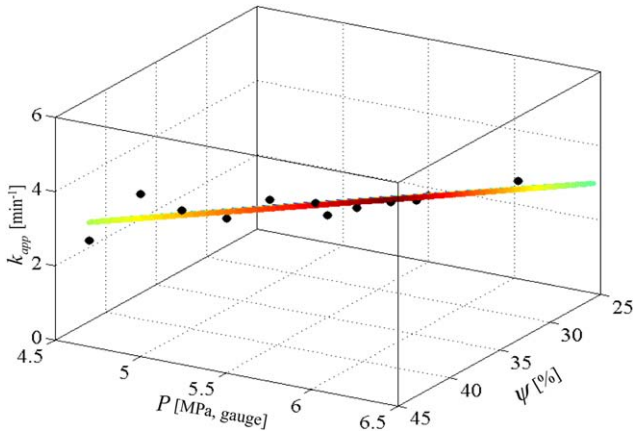

Figure 9. Relationships among the apparent kinetic constant, pressure, and initial mass fraction of *n*-tetradecane in the slurry (*T* =~277.6 K; impeller speed = 600 rpm).

[Color figure can be viewed in the online issue, which is available at wileyonlinelibrary.com.]

By replacing $\frac{1}{\frac{1}{k_{hg}A^{p}}+\frac{\Delta H_e+D\Delta H_u-D\Delta H_{hg}}{\Delta H_e+D\Delta H_u+D\Delta H_a}\frac{1}{k_{tra}A^{g-w}}}$ with the apparent kinetic constant of hydrate growth k_{app}, Eq. 18 can be rewritten as

$$r_{hg} = k_{app}\left((c)_w^{sat}-(c)_w^{eq}\right) \tag{19}$$

where

$$(c)_w^{sat} = c_w\frac{f(T,P)}{H(T,P)} \tag{20}$$

$$(c)_w^{eq} = c_w\frac{f(T,P^{eq})}{H(T,P^{eq})} \tag{21}$$

c_w is the density of water. The fugacity of methane, f, was calculated through the Peng–Robinson equation of state.[25] Henry's law constant, H, was calculated using an equation given by Mohebbi et al.[30]

Figure 9 shows the apparent kinetic constants for various experimental conditions. These constants were obtained by fitting Eq. 19 to the kinetic data for the first stage using the least squares method and are listed in Table 2. In Figure 9, a plane was fitted to these constants. The plane is expressed as

$$k_{app} = C_1\psi+C_2P+C_3 \tag{22}$$

where $C_1 = 0.127$ (% min)$^{-1}$, $C_2 = 1.224$ (MPa min)$^{-1}$, $C_3 = -8.138$ min^{-1}, and ψ is the initial mass fraction of *n*-tetradecane in the slurry.

Substituting Eq. 22 into Eq. 19 yields

$$r_{hg} = (C_1\psi+C_2P+C_3)\left((c)_w^{sat}-(c)_w^{eq}\right) \tag{23}$$

Equation 23 can be used to predict the rate of hydrate growth in the first stage.

The quantities of methane enclathrated in hydrates at the end of the first stage were approximately 0.019, 0.021, and 0.018 mol for the 1#, 2#, and 3# slurries, respectively. Then, the time, excluding the induction time, for the sudden increase in the hydrate growth rate can be calculated using Eq. 24

$$t_1 = \frac{B}{V_w^0(C_1\psi+C_2P+C_3)\left((c)_w^{sat}-(c)_w^{eq}\right)} \tag{24}$$

where B is a constant for a certain slurry and equals 0.019, 0.021, and 0.018 mol for the 1#, 2#, and 3# slurries, respectively.

The second stage begins after t_1. It is supposed that the mass-transfer resistance of methane from the bulk water droplet to the hydrate-particle surface is negligible, as compared with the resistance lying in the space between the bulk liquid *n*-tetradecane and the bulk water droplet. Then, at steady state, the transfer rate of methane from the bulk liquid *n*-tetradecane to the bulk water droplet, r_{tra}, equals the rate of hydrate growth in the second stage. The transfer rate is

$$r_{tra} = k_{tra}A^{w-o}\left(s(c)_o^{b}-(c)_w^{b}\right) = k_{tra}A^{w-o}\left(s(c)_o^{sat}-(c)_w^{b}\right) \tag{25}$$

where k_{tra} is the mass-transfer coefficient of methane from the bulk liquid *n*-tetradecane to the bulk water droplet, A^{w-o} is the water-liquid *n*-tetradecane interfacial area per unit volume of water, $(c)_o^{b}$ is the concentration of methane in the bulk liquid *n*-tetradecane, $(c)_o^{sat}$ is the saturation concentration of methane in the liquid *n*-tetradecane at the experimental pressure and temperature, and s is the equilibrium partition coefficient of methane between water and liquid *n*-tetradecane at the experimental pressure and temperature.

Equating r_{hg} in Eq. 17 and r_{tra} in Eq. 25 yields

$$r_{hg} = \frac{1}{\frac{1}{k_{hg}A^{p}}+\frac{1}{k_{tra}A^{w-o}}}\left(s(c)_o^{sat}-(c)_w^{eq}\right) \tag{26}$$

Table 2. Summary of the Results of the Experiments in the Presence of the Solid Particles of *n*-Tetradecane (*T* = ~277.6 K; Impeller Speed = 600 rpm)

Run	*P* (MPa, Gauge)	ψ (%)	Induction Time (min)	k_{app} (min^{-1})	$k_{hg}A_1^{p}\times10^{-4}$ (min^{-1})	$k_{tra}A^{w-o}$ (min^{-1})	*j*
1	4.70[a]	45	4	2.867	–	–	–
2	5.00	45	5	4.369	5.5	10.4	−23.6
3	5.24	45	0	4.135	1.1	5.3	−40.9
4	5.75	45	4	4.884	6.0	8.4	−24.7
5	6.26	45	3	5.110	8.3	8.2	−36.9
6	6.46	45	4	5.432	8.7	7.3	−13.9
7	5.50	25	4	1.776	5.4	3.2	−68.0
8	5.50	35	0	2.744	5.2	6.7	−29.3
9	5.50	45	4	4.150	4.3	8.9	−27.4
10	6.02	25	3	2.629	3.1	3.3	−56.0
11	6.02	35	0	3.593	9.9	5.1	−35.6
12	6.02	45	0	5.035	1.5	5.4	−31.4

[a]The rate of hydrate growth under a pressure of 4.70 MPa (gauge) showed no sudden increase because of a small driving force.

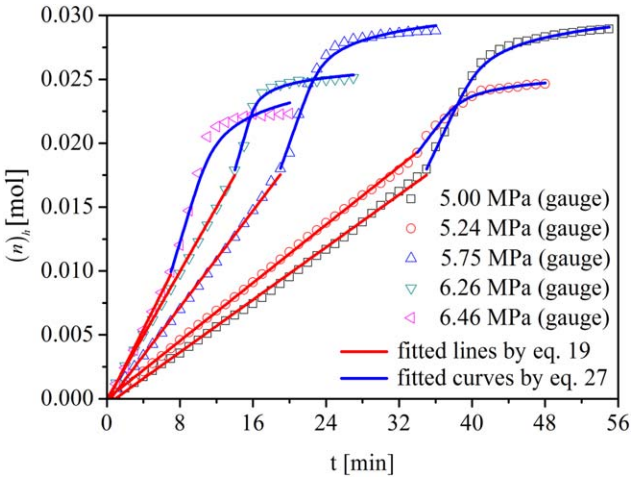

Figure 10. Moles of methane enclathrated in hydrates at various pressures (ψ = 45 wt %; T = ~277.6 K; impeller speed = 600 rpm).

[Color figure can be viewed in the online issue, which is available at wileyonlinelibrary.com.]

It is supposed that $k_{tra}A^{w-o}$ in Eq. 26 remains constant throughout the second stage. Let $A^p = A_1^p\left(\frac{(n)_h}{(n)_{h,1}}\right)^j$. Then, Eq. 26 can be rewritten as

$$r_{hg} = \frac{1}{\frac{1}{k_{hg}A_1^p\left(\frac{(n)_h}{(n)_{h,1}}\right)^j} + \frac{1}{k_{tra}A^{w-o}}}\left(s(c)_o^{sat} - (c)_w^{eq}\right) \tag{27}$$

where A_1^p and $(n)_{h,1}$ are the surface area of hydrate particles per unit volume of water and the molar number of methane enclathrated in hydrates at the onset of the second stage, respectively; and j is the exponential term. $(c)_o^{sat}$ and s were obtained by the thermodynamic flash calculations using the Peng–Robinson and the PSRK equations of state, respectively.

Influence of pressure on the rate of hydrate growth

Figure 10 shows the moles of methane enclathrated in hydrates at various pressures. In the figure, the zero time point represents the onset of hydrate growth. The experimental data for the second stage in Figure 10 were calculated by a method similar to that provided in the data interpretation section, treating liquid *n*-tetradecane as the continuous phase. Equation 27 was fitted to these data by the least squares method and the fourth-order Runge–Kutta method. The fitting parameters are listed in Table 2.

In Figure 10, the growth rate in the first stage increased with increased pressure. There were two effects that could lead to this trend. First, Table 2 shows that the apparent kinetic constant in the 3# slurry increased with the pressure except for the case under a pressure of 5.00 MPa (gauge). This increasing tendency for the apparent kinetic constant could be interpreted from the increase in A^{g-w} as the pressure was increased. Second, the thermodynamic driving force was similarly increased.

A noticeable trend for the growth rates in the second stage under various pressures was not observed in Figure 10, which could be understood from the fitting parameters in Table 2. At the onset of the second stage, the values of $k_{hg}A_1^p$ were approximately four orders of magnitude larger than those of $k_{tra}A^{w-o}$, which indicated that the growth rates were controlled by the mass transfer of methane from the liquid *n*-tetradecane to the water. The negative values of j implied decreases in the surface area of growing hydrates because of agglomeration between the hydrates. When the surface area decreased to a certain point, crystal growth began to influence the rates. The j values showed no obvious changing trend with the pressure. Therefore, the growth rates in the second stage varied irregularly at different pressures.

Influence of the initial mass fraction of n-tetradecane on the rate of hydrate growth

Figure 11 shows the moles of methane enclathrated in hydrates for various initial mass fractions of *n*-tetradecane in the slurries. The experimental data in Figure 11 were obtained by the same method used for the experimental data in Figure 10. In Figure 11, the rates of hydrate growth in the first stage at both 5.50 and 6.02 MPa (gauge) increased as the initial fraction was increased from 25 to 45 wt %. This tendency could be attributed to the increased heat removal rate and $k_a A^{g-w}$, with more solid particles of *n*-tetradecane in the slurry prior to hydrate formation.

For runs 7–9 and runs 10–12 in Table 2, the value of j increased with the increasing initial mass fraction of *n*-tetradecane, which demonstrated that the agglomeration was more serious in the slurry with a higher mass fraction of water.

Comparisons of the induction times and the hydrate growth rates

To evaluate the effect of the addition of the PCM particles, two experiments in which hydrates were formed in pure water and an w/o emulsion were conducted. The gas consumption curves for the two experiments are the same as that plotted in Turner et al.[10] and not discussed in detail. The induction times and the growth rates obtained in the two experiments, as well as those achieved with the PCM particles, are listed in Table 3 for comparison. The induction times shown in Table 2 were much shorter than those listed in Table 3 in the absence of the PCM particles because the particles promoted the nucleation of hydrates. The comparison of the growth rate in Table 3 was based on approximately the same degree of deviation from

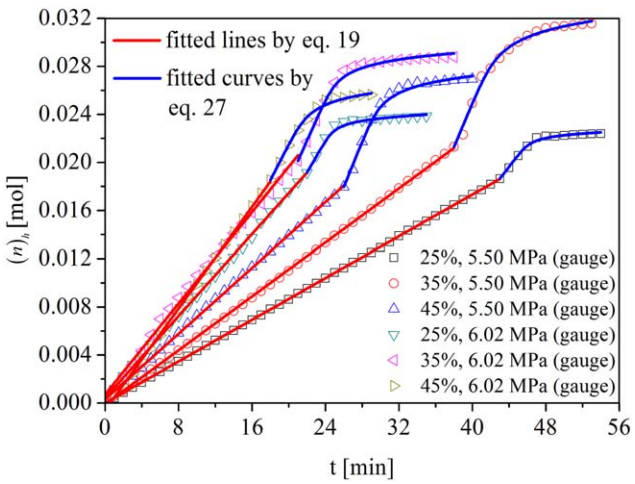

Figure 11. Moles of methane enclathrated in hydrates for various initial mass fractions of *n*-tetradecane in the slurries (T =~277.6 K; impeller speed = 600 rpm).

[Color figure can be viewed in the online issue, which is available at wileyonlinelibrary.com.]

Table 3. Comparisons of the Induction Times and the Hydrate Growth Rates

		P (MPa, Gauge)	T (K)	F	Impeller Speed (rpm)	φ (%)	Induction Time (min)	r_{hg} (mol/(min m^3))
(1a)	This work[a]	5.00	277.6	1.24	600	100	5	68.20
(1b)	This work[b]	5.00	277.6	1.24	600	100	189	13.52
(1c)	Turner et al.[10]	4.92	277.2	1.27	600	100	10.4	17.20
(2a)	This work[a]	5.00	277.6	1.24	600	38	5	198.60
(2b)	This work[c]	5.00	277.6	1.24	600	38	102	20.13
(2c)	Turner et al.[10]	4.92	277.2	1.27	500	35	19.9	23.49

[a]In the 3# slurry.
[b]In pure water.
[c]In an w/o emulsion.

equilibrium and volume fraction of water in the slurry. Considering that the volume fraction of water varied with time, instantaneous growth rates were compared. In the first group, the growth rate in the 3# slurry at the beginning of the first stage, when *n*-tetradecane existed as solid particles, was nearly four times higher than that in pure water, and quadruple that reported in Turner et al.[10] at φ of 100%. In the second group, the growth rate of the second stage in the 3# slurry at F of 1.24 and φ of 38% was approximately nine times higher than that in the w/o emulsion, and eight times that reported in Turner et al.[10] at F of 1.27 and φ of 35%. In addition, it can be seen that the growth rate in the slurry containing water and the PCM particles (1a in Table 3) was approximately two times larger than that in the w/o emulsion (2b in Table 3).

The comparison results indicated that the growth rates of methane hydrate were greatly enhanced using solid *n*-tetradecane to directly remove the heat released during hydrate growth. The actual hydrate-forming temperature is closely related to the rate of heat transfer in the hydrator and more closely approximates the experimental temperature with a higher heat-transfer rate. The rate of direct heat removal is much higher than that of indirect heat removal because of the large area for heat transfer and the absence of resistance to the heat conduction through the wall of the hydrator. It follows that the actual thermodynamic driving force for hydrate growth under direct heat removal is larger than that under indirect heat removal. Therefore, the growth rates obtained under direct heat removal were much higher than those under indirect heat removal.

Conclusions

Methane hydrate formation under direct heat removal by the phase change of solid *n*-tetradecane were researched. The induction time was only 3–5 min and sometimes was even less than 1 min. The hydrate growth rates obtained with the PCM particles were approximately three to nine times larger than those achieved under indirect heat removal at approximately the same degree of deviation from equilibrium and volume fraction of water in the slurry. The growth period at the presence of the PCM particles occurred in two stages. The growth rate in the first stage was practically constant and increased with the pressure and initial mass fraction of *n*-tetradecane in the slurry. The second stage was identified by a sudden growth rate increase, which was considered to be caused by an inversion of the continuous phase in the slurry from the water to the liquid *n*-tetradecane. The two proposed models fitted the experimental data for the two stages well. The model for the first stage can be used to predict the growth rate and the time for conversion of the first stage into the second stage. The fitting parameters for the second stage indicated that the growing hydrates seriously agglomerated. The influence of crystal growth on the hydrate-growth rate gradually became significant as a result of the agglomeration. A method of improving both mass and heat transfer will be considered to further enhance the hydrate growth rate in future work.

Acknowledgment

The financial support received from the National Basic Research Program of China (973 Program, No. 2012CB215005) and the China-Europe Small- and Medium-Sized Enterprises Energy Saving and Carbon Reduction Research Project (No. SQ2013ZOA100002) is greatly appreciated.

Notation

A = area per unit volume of water, m^2/m^3
B = constant, mol
c = concentration, mol/m^3
C_1 = constant, (% min)$^{-1}$
C_2 = constant, (MPa min)$^{-1}$
C_3 = constant, min^{-1}
$(c)_i$ = concentration of methane in phase i, mol/m^3
D = molar ratio of methane to *n*-tetradecane in the *n*-tetradecane solution saturated with methane under the experimental pressure and temperature, mol/mol
f = fugacity, MPa
F = degree of deviation from equilibrium
H = Henry's law constant, MPa
ΔH = enthalpy change, kJ/mol
j = exponential term
k = mass-transfer coefficient, m/min
k_{hg} = kinetic constant of hydrate growth, m/min
k_{app} = apparent kinetic constant of hydrate growth, min^{-1}
M = molecular weight, kg/mol
N = hydration number
n = moles, mol
$(n)_i$ = moles of methane in phase i, mol
P = pressure, MPa (gauge)
Q = heat, kJ
r = rate, mol/(min m^3)
R = gas constant, J/(mol K)
s = equilibrium partition coefficient of methane between water and liquid *n*-tetradecane under the experimental pressure and temperature, m^3/m^3
t = time, min
T = temperature, K
V = volume, m^3
Z = gas compressibility factor

Greek letters

φ = volume fraction of water in the slurry, %
ρ = density, kg/m^3
ψ = initial mass fraction of *n*-tetradecane in the slurry, %

Superscripts and subscripts

0 = the state when the hydrate growth begins
1 = the state when the rate of hydrate growth suddenly increases

a = absorption of methane in water
b = bulk
e = fusion of solid particles of *n*-tetradecane
eq = equilibrium under the experimental temperature and the methane-water-hydrate equilibrium pressure
g−w = methane-water interface
g−o = methane-liquid *n*-tetradecane interface
h = methane hydrate
hg = growth of methane hydrate
MeC = total methane that flowed through the mass flow controller
MeM = total methane that flowed through the mass flow meter
o = liquid *n*-tetradecane
p = hydrate particles
sat = condition of saturation
tra = transfer of methane from the liquid *n*-tetradecane to the water
u = transfer of methane from the water to the liquid *n*-tetradecane
w = water
w−o = water-liquid *n*-tetradecane interface

Literature Cited

1. Hu YH, Ruckenstein E. Clathrate hydrogen hydrate—a promising material for hydrogen storage. *Angew Chem Int Ed*. 2006;45:2011–2013.
2. Kumar R, Linga P, Moudrakovski I, Ripmeester JA, Englezos P. Structure and kinetics of gas hydrates from methane/ethane/propane mixtures relevant to the design of natural gas hydrate storage and transport facilities. *AIChE J*. 2008;54:2132–2144.
3. Lee H, Seo Y, Seo YT, Moudrakovski IL, Ripmeester JA. Recovering methane from solid methane hydrate with carbon dioxide. *Angew Chem Int Ed*. 2003;42:5048–5051.
4. Lee HJ, Lee JD, Linga P, Englezos P, Kim YS, Lee MS, Kim YD. Gas hydrate formation process for pre-combustion capture of carbon dioxide. *Energy*. 2010;35:2729–2733.
5. Eslamimanesh A, Mohammadi AH, Richon D, Naidoo P, Ramjugernath D. Application of gas hydrate formation in separation processes: a review of experimental studies. *J Chem Thermodyn*. 2012;46:62–71.
6. Park KN, Hong SY, Lee JW, Kang KC, Lee YC, Ha MG, Lee JD. A new apparatus for seawater desalination by gas hydrate process and removal characteristics of dissolved minerals (Na^+, Mg^{2+}, Ca^{2+}, K^+, B^{3+}). *Desalination*. 2011;274:91–96.
7. Englezos P, Kalogerakis N, Dholabhai PD, Bishnoi PR. Kinetics of gas hydrate formation from mixture of methane and ethane. *Chem Eng Sci*. 1987;42:2659–2666.
8. Englezos P, Kalogerakis N, Dholabhai PD, Bishnoi PR. Kinetics of formation of methane and ethane gas hydrates. *Chem Eng Sci*. 1987;42:2647–2658.
9. Skovborg P, Rasmussen P. A mass transfer limited model for the growth of methane and ethane gas hydrates. *Chem Eng Sci*. 1994;49:1131–1143.
10. Turner DJ, Miller KT, Sloan ED. Methane hydrate formation and an inward growing shell model in water-in-oil dispersions. *Chem Eng Sci*. 2009;64:3996–4004.
11. Mochizuki T, Mori YH. Clathrate-hydrate film growth along water/hydrate-former phase boundaries numerical heat-transfer study. *J Cryst Growth*. 2006;290:642–652.
12. Gupta A, Lachance J, Sloan ED, Koh CA. Measurements of methane hydrate heat of dissociation using high pressure differential scanning calorimetry. *Chem Eng Sci*. 2008;63:5848–5853.
13. Pang WX, Chen GJ, Dandekar A, Sun CY, Zhang CL. Experimental study on the scale-up effect of gas storage in the form of hydrate in a quiescent reactor. *Chem Eng Sci*. 2007;62:2198–2208.
14. Yang DL, Le LA, Martinez RJ, Currier RP, Spencer DF. Kinetics of CO_2 hydrate formation in a continuous flow reactor. *Chem Eng J*. 2011;172:144–157.2
15. Falenty A, Salamatin AN, Kuhs WF. Kinetics of CO_2-hydrate formation from ice powders: data summary and modeling extended to low temperatures. *J Phys Chem C*. 2013;117:8443–8457.
16. Susilo R, Ripmeester JA, Englezos P. Methane conversion rate into structure H hydrate crystals from ice. *AIChE J*. 2007;53:2451–2460.
17. Isobe F, Mori YH. Formation of gas hydrate or ice by direct-contact evaporation of CFC alternatives. *Int J Refrig*. 1992;115:137–142.
18. Mori T, Mori YH. Characterization of gas hydrate formation in direct-contact cool storage process. *Int J Refrig*. 1989;12:259–265.
19. Huang L, Petermann M, Doetsch C. Evaluation of paraffin/water emulsion as a phase change slurry for cooling applications. *Energy*. 2009;34:1145–1155.
20. Gschwander S, Schossig P, Henning HM. Micro-encapsulated paraffin in phase-change slurries. *Sol Energy Mater Sol C*. 2005;89:307–315.
21. Lu W, Tassou SA. Experimental study of the thermal characteristics of phase change slurries for active cooling. *Appl Energy*. 2012;91:366–374.
22. Parrish WR, Prausnitz JM. Dissociation pressures of gas hydrates formed by gas mixtures. *Ind Eng Chem Proc Des Dev*. 1972;11:26–35.
23. Tulk CA, Ripmeester JA, Klug DD. The application of Raman spectroscopy to the study of gas hydrates. *Gas Hydrates: Chall Future*. 2000;912:859–872.
24. Naghibi H, Dec SF, Gill SJ. Heat of solution of methane in water from 0 to 50°C. *J Phys Chem*. 1986;90:4621–4623.
25. Peng DY, Robinson DB. A new two-constant equation of state. *Ind Eng Chem Fundam*. 1976;15:59–64.
26. Ballard AL, Sloan ED. The next generation of hydrate prediction III: Gibbs energy minimization formalism. *Fluid Phase Equilib*. 2004;218:15–31.
27. Huang L, Günther E, Doetsch C, Mehling H. Subcooling in PCM emulsions—part 1: experimental. *Thermochim Acta*. 2010;509:93–99.
28. Roy SK, Avanic BL. Laminar forced convection heat transfer with phase change material emulsions. *Int Commun Heat Mass Transf*. 1997;24:653–662.
29. Karpinski PH. Crystallization as a mass transfer phenomenon. *Chem Eng Sci*. 1980;35:2321–2324.
30. Mohebbi V, Naderifar A, Behbahani RM, Moshfeghian M. Determination of Henry's law constant of light hydrocarbon gases at low temperatures. *J Chem Thermodyn*. 2012;51:8–11.

Manuscript received Jan. 8, 2015, and revision received Apr. 21, 2015.